J Infrared Milli Terahz Waves (2009) 30:8–25
DOI 10.1007/s10762-008-9418-x

Calculation of Radiation from a Helically Cut Waveguide for a Gyrotron Mode Converter in the Quasi-Optical Approximation

E. M. Choi · M. A. Shapiro · J. R. Sirigiri · R. J. Temkin

Received: 25 June 2008 / Accepted: 28 August 2008 /
Published online: 18 September 2008

Abstract We present results of calculations of the radiation from a helically cut waveguide launcher, a so-called Vlasov launcher, which is commonly used either internal or external to a gyrotron for purposes of mode conversion. A gyrotron internal mode converter consists of such a launcher that radiates the waveguide mode as a nearly Gaussian beam in free space followed by a set of mirrors to focus and direct the radiation. The radiation from the launcher is first calculated using a geometric optics representation of the waveguide mode. Then the radiation is calculated in the quasi-optical limit, including diffraction. These analytic results are compared to a rigorous calculation using the computer code SURF3D, which uses an electric field integral equation (EFIE) approach. Good agreement is obtained between the quasi-optical theory and the SURF3D calculation. The present results provide new insights into the accuracy of the quasi-optical theory and may be useful for the design and improvement of Vlasov-type mode converters.

Keywords Mode converter · Vlasov launcher · Gyrotron · Quasi-optical approximation

1 Introduction

High power gyrotron cavities operate in high order transverse electric (TE) modes of a circular waveguide [1, 2]. It is important to convert these high order TE modes into a low order waveguide mode or a Gaussian-like beam in free space in order to reduce losses in the transmission of the gyrotron output power. Present day gyrotrons

E. M. Choi · M. A. Shapiro (✉) · J. R. Sirigiri · R. J. Temkin
Plasma Science & Fusion Center, Massachusetts Institute of Technology,
167 Albany St., Bldg. NW 16, Cambridge, MA 02139, USA
e-mail: shapiro@psfc.mit.edu

operating at power levels of watts to above one megawatt use a mode converter located inside the gyrotron, a so-called internal mode converter (IMC).

An internal mode converter consisting of a launcher followed by a set of smooth focusing mirrors was first proposed and demonstrated by Vlasov *et al.* [3]. The launcher is a helically cut section of waveguide. A step-wise waveguide cut can be used for axially-symmetrical waveguide modes. The advantage of this version of the IMC is that it is relatively simple and is very compact. The disadvantage is that the power radiated from the launcher contains sidelobes, which limit the IMC efficiency to about 80%. This low efficiency is unacceptable for megawatt power level gyrotrons. However, the Vlasov IMC is used in low power gyrotrons because it is very compact and easy to fabricate [4]. It is also used external to the gyrotron [5, 6].

The Vlasov antenna has the advantage of simple construction, but the disadvantage of modest efficiency. Several major improvements to the Vlasov antenna and improved concepts for quasi-optical antennas have been reported in the literature [7–13]. These new approaches allow one to improve the efficiency of conversion of a rotating circular waveguide mode into a Gaussian beam. In one of the most successful of these designs, a mixture of modes is generated by a rippled wall prior to the launcher so as to form a Gaussian-like beam with little or no sidelobes, thus allowing very high efficiency in the IMC [11]. The launcher has been optimized numerically using the surface current integral equation method, leading to close to 100% theoretical efficiency for the IMC [14]. However, for gyrotrons of low to moderate power levels, less than some kilowatts or tens of kilowatts of power, the simplicity of the Vlasov IMC outweighs the disadvantage of lower efficiency. The present paper is intended to give new insight into the design of the Vlasov IMC and thus help in optimizing that design.

In this paper, we use the quasi-optical theory of diffraction to calculate the radiation from a helical cut of a waveguide. The case considered applies to the Vlasov launcher and the Vlasov IMC. Analytic results are compared to numerical results obtained from the electric field integral equation method [14]. Since the Vlasov IMC is still in use, the present results should be helpful in designing such converters. They can be used in very high frequency (up to THz) gyrotrons for dynamic nuclear polarization (DNP) NMR spectroscopy or plasma diagnostics, where the 80% conversion efficiency is acceptable.

Figure 1 shows a schematic of a CW millimeter wave gyrotron at MIT that uses a Vlasov-type IMC; the present theory can be used to improve the design of such a Vlasov IMC. Vlasov launchers are also used as external mode converters for gyrotrons [5, 6] or as launchers for electron cyclotron plasma heating. In many cases, these Vlasov launchers are designed based on simple geometric optics. The present theory, which includes diffraction, should lead to improved designs of these Vlasov converters. In addition, this paper compares the results of the quasi-optical theory with more rigorous results from the surface current integral equation method, yielding new insights into the accuracy of the quasi-optical approach.

The quasi-optical theory of diffraction presented in this paper can also be used for the preliminary design and optimization of the launchers of gyrotron internal mode converters while the final design can be improved, finalized and verified by numerical codes. The present results will also be useful for understanding the general role of edge diffraction in the gyrotron IMC design. The etalon problems of diffraction theory for waveguide launchers have been presented [15–17]. This

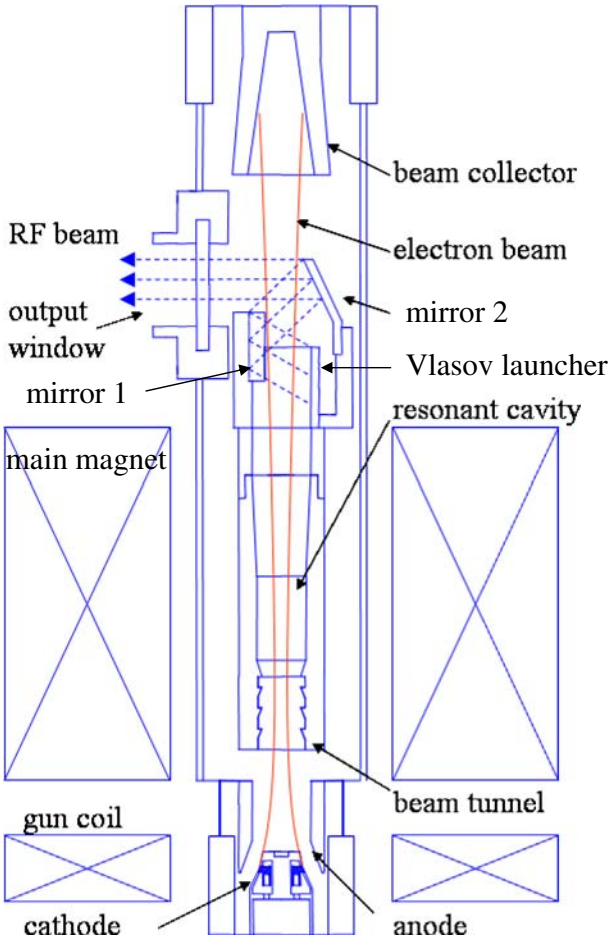

Fig. 1 Schematic drawing of a gyrotron in cross-sectional view (not shown to scale). The basic components of the gyrotron include a magnet, an electron gun, and a vacuum tube which consists of a beam tunnel, a resonator, a mode converter and a collector. The Vlasov IMC consists of a Vlasov launcher and two mirrors.

paper demonstrates a simple approach of how this diffraction theory is applied to a Vlasov launcher. This approach can be improved using the higher order terms in the etalon diffraction problem solution [16]. The quasi-optical approach used in this paper was previously applied to radiowave propagation in the atmosphere and later was extended to optical and millimeter wave applications [16, 18–20].

2 Geometrical optics representation for a waveguide mode

In this section we derive an analytic theory for designing the launcher. The theory is based on a geometric optics representation of wave propagation in overmoded structures. The geometrical optics of waveguide mode converters is presented in [10]. The goal of such an analysis is to present a more physical picture of the process of radiation from a launcher which is essential to optimize the performance of the launcher. To improve upon the basic geometric representation we incorporate the

effects of diffraction by using a quasi-optical representation of the rays in Sections 3 and 4. Diffraction effects are very important in open waveguides which have finite wall thickness at the open end and especially in a helically cut launcher with a sharp tip which is the subject of this paper.

Figure 1 shows a schematic of a CW millimeter wave gyrotron at MIT used for dynamic nuclear polarization (DNP) / NMR experiments. The gyrotron is installed in a superconducting magnet. The electron beam is generated by a magnetron injection gun (MIG). The IMC is located after the cavity and operates in a waveguide just above cutoff, thus reducing the size and increasing the efficiency of the converter. The converter is constructed of a Vlasov launcher, which radiates the power from the waveguide TE mode into an rf beam, followed by two mirrors that direct the rf beam to the output window.

For a TE waveguide mode, the Helmholtz equation for the axial magnetic field $u = H_z$ is written in cylindrical coordinates (r, ϕ) as

$$\frac{\partial^2 u}{\partial r^2} + \frac{1}{r}\frac{\partial u}{\partial r} + \frac{1}{r^2}\frac{\partial^2 u}{\partial \varphi^2} + k_\perp^2 u = 0, \tag{1}$$

$k_\perp = \sqrt{k^2 - k_z^2}$ is the transverse wave number, where k is the wave number and k_z is the axial wave number. The solution for TE_{mn} modes is

$$u = J_m(k_\perp r)e^{-im\varphi} \tag{2}$$

where m is the azimuthal index.

The geometrical optics solution can be derived within the approximation $k_\perp r \gg 1$, $m \gg 1$. We represent the solution of Eq. 1 as $u = A(r)e^{-ik_\perp s(r,\varphi)}$, where $k_\perp$ is a large parameter. The second order terms of $k_\perp$ give an eikonal equation,

$$\left(\frac{\partial s}{\partial r}\right)^2 + \frac{1}{r^2}\left(\frac{\partial s}{\partial \varphi}\right)^2 = 1 \tag{3}$$

and the function $s(r, \varphi)$ is an eikonal. The first order term of $k_\perp$ gives the transfer equation as shown below

$$2\frac{\partial A}{\partial r}\frac{\partial s}{\partial r} + \left(\frac{\partial^2 s}{\partial r^2} + \frac{1}{r}\frac{\partial s}{\partial r} + \frac{1}{r^2}\frac{\partial^2 s}{\partial \varphi^2}\right) A = 0. \tag{4}$$

Assuming $s(r, \varphi) = f(r) + \frac{m\varphi}{k_\perp}$, we obtain from Eq. 3

$$\begin{aligned} f(r) &= \int \sqrt{1 - \frac{m^2}{k_\perp^2 r^2}}\, dr \\ &= \sqrt{r^2 - \frac{m^2}{k_\perp^2}} - \frac{m}{k_\perp} \arccos\left(\frac{m}{k_\perp r}\right). \end{aligned}$$

Therefore, the eikonal is

$$s(r, \varphi) = \sqrt{r^2 - \frac{m^2}{k_\perp^2}} + \frac{m}{k_\perp}\left(\varphi - \arccos\left(\frac{m}{k_\perp r}\right)\right). \tag{5}$$

From Eq. 4 we obtain the amplitude

$$A(r) = \left(r^2 - \frac{m^2}{k_\perp^2}\right)^{-1/4}. \tag{6}$$

The geometrical interpretation of the solutions of Eqs. 5, 6 is that the density of rays that are tangential to the caustic whose radius is $r_c = \frac{m}{k_\perp}$ tends to go to infinity as r goes to r_c. That is why the amplitude Eq. 6 goes to infinity at the caustic.

The equation of a ray can be expressed as

$$\vartheta = \varphi - \arccos\left(\frac{r_c}{r}\right) = const. \tag{7}$$

The equation of constant phase (eikonal) is given by

$$s(r,\varphi) = \sqrt{r^2 - \frac{m^2}{k_\perp^2}} + \frac{m}{k_\perp}\left(\varphi - \arccos\left(\frac{m}{k_\perp r}\right)\right) = const. \tag{8}$$

The surfaces $s = const$ are the evolvents of the caustic shown in Fig. 2. They are perpendicular to the rays $\vartheta = const$ in every point.

The geometrical optics representation Eqs. 5, 6 correspond to the Debye approximation for the Hankel function,

$$H_m^{(2)}(k_\perp r)e^{-im\varphi} \sim \frac{1}{\sqrt[4]{r^2 - \frac{m^2}{k_\perp^2}}} exp\left(-ik_\perp\sqrt{r^2 - \frac{m^2}{k_\perp^2}} - im\left(\varphi - \arccos\left(\frac{m}{k_\perp r}\right)\right) + i\frac{\pi}{4}\right). \tag{9}$$

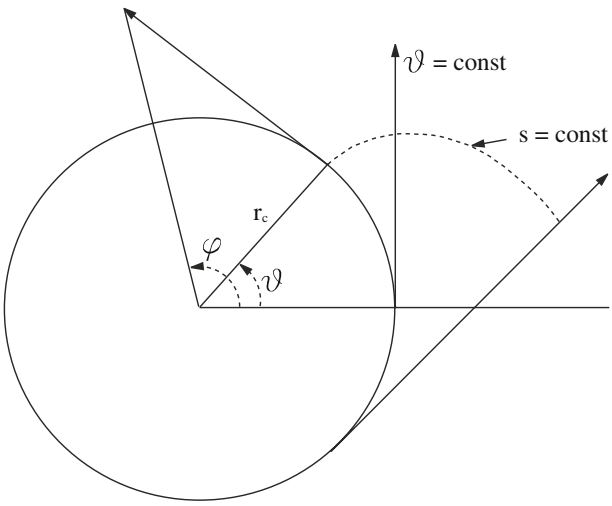

Fig. 2 The representation of ray coordinates.

The TE_{mn} mode field distribution is a superposition of the outgoing and incoming cylindrical waves:

$$J_m(k_\perp r) = \frac{1}{2}\left(H_m^{(1)}(k_\perp r) + H_m^{(2)}(k_\perp r)\right) \sim \frac{1}{\sqrt[4]{r^2 - \frac{m^2}{k_\perp^2}}} \cos\left(k_\perp\sqrt{r^2 - \frac{m^2}{k_\perp^2}} - m\arccos\left(\frac{m}{k_\perp r}\right) - \frac{\pi}{4}\right) \tag{10}$$

3 Quasi-optical representation in ray coordinates

In this section, diffraction will be added to the previously developed description of the geometric optics. This is also called the 'quasi-optical' representation. Diffusion of light rays occurs due to edge diffraction into the region where rays are not present in a geometrical optics calculation. It is worth representing the diffraction theory in the ray coordinates. We transform the Helmholtz equation, Eq. 1, to the ray coordinates (s,ϑ) using Eqs. 7, 8.

The Helmholtz equation in the ray coordinates can be expressed as below

$$\frac{\partial^2 u}{\partial s^2} + \frac{\partial u}{\partial s}\frac{1}{(s - r_c\vartheta)} + \frac{\partial^2 u}{\partial \vartheta^2}\frac{1}{(s - r_c\vartheta)^2} + \frac{\partial u}{\partial \vartheta}\frac{r_c}{(s - r_c\vartheta)^3} + k_\perp^2 u = 0. \tag{11}$$

We convert the Helmholtz equation (Eq. 11) into a parabolic equation in the ray coordinates. So as to convert it, we represent u as

$$u = A(s,\vartheta)e^{-ik_\perp s}.$$

Assuming that $k_\perp$ is a large parameter, we drop the terms $\frac{\partial^2 A}{\partial s^2}$ and $\frac{\partial A}{\partial s}\frac{1}{(s-r_c\vartheta)}$ which are small compared to $-2ik_\perp\frac{\partial A}{\partial s}$ and $\frac{-ik_\perp}{(s-r_c\vartheta)}A$, respectively. Therefore, Eq. 11 can be expressed as [19]

$$-2ik_\perp\frac{\partial A}{\partial s} - \frac{ik_\perp}{(s - r_c\vartheta)}A + \frac{1}{(s - r_c\vartheta)^2}\frac{\partial^2 A}{\partial \vartheta^2} + \frac{r_c}{(s - r_c\vartheta)^3}\frac{\partial A}{\partial \vartheta} = 0. \tag{12}$$

We introduce $X = \sqrt{\alpha}s$, $Y = \alpha(s - r_c\vartheta)^2$. Equation 12 is transformed to

$$-i\frac{\partial A}{\partial X} - 2i\sqrt{Y}\frac{\partial A}{\partial Y} - i\frac{1}{2\sqrt{Y}}A + 2\alpha^{3/2}r_c^2\frac{1}{k_\perp}\frac{\partial^2 A}{\partial Y^2} = 0. \tag{13}$$

We define α such that the coefficient of $\frac{\partial^2 A}{\partial Y^2}$ is 1

$$\alpha = \left(\frac{k_\perp}{2r_c^2}\right)^{2/3}. \tag{14}$$

We express A as follows

$$A = B(X,Y)exp\left(i\frac{2}{3}Y^{3/2}\right). \tag{15}$$

Therefore Eq. 13 can be rewritten as

$$-i\frac{\partial B}{\partial X}+\frac{\partial^2 B}{\partial Y^2}+YB=0. \tag{16}$$

Equation 16 then can be solved using separation of variables

$$B(X,Y)=e^{-itX}D(Y), \tag{17}$$

$$\frac{d^2D}{dY^2}-(t-Y)D=0. \tag{18}$$

The solution of Eq. 18 is a superposition of Airy functions $Ai(t-Y)$ and $Bi(t-Y)$

$$D(Y)=w_2(t-Y)=Bi(t-Y)-iAi(t-Y). \tag{19}$$

Going back to the coordinates ϑ and $l=s-r_c\vartheta=\sqrt{r^2-r_c^2}$, we represent the solution of Eq. 12 using Eqs. 14, 15, 17 and 19 as follows

$$A=exp\left(-it\sqrt{\alpha}(l+r_c\vartheta)\right)\cdot w_2(t-\alpha l^2)\cdot exp\left(i\frac{2}{3}\alpha^{3/2}l^3\right). \tag{20}$$

A general solution of Eq. 12 can be constructed as a superposition of the fields (20) with different variables t.

Equation 20 is the quasi-optical representation of fields along the ray. To compare it with the geometrical optics representation, we use the asymptotic representation for the Airy function. To derive the asymptotics we use the following equation [18]

$$\begin{aligned} w_2(-z) &= Bi(-z)-iAi(-z)\\ &= \frac{-i}{\pi}\int_0^\infty e^{i\left(\frac{p^3}{3}-zp\right)}dp+\frac{1}{\pi}\int_0^\infty e^{-\frac{p^3}{3}-zp}dp \end{aligned} \tag{21}$$

where the second term is small for large $z>0$. We calculate the asymptotics of the first integral in Eq. 21 using the method of stationary phase. The phase function is

$$\phi(p)=\frac{p^3}{3}-pz.$$

The stationary point is determined by the equation

$$\frac{d\phi}{dp}=0.$$

Therefore, the stationary point is represented as $p_{st}=\sqrt{z}$. The phase function is represented as

$$\phi(p)=\phi(p_{st})+\frac{1}{2}\frac{d^2\phi}{dp^2}|_{p_{st}}(p-p_{st})^2=-\frac{2}{3}z^{3/2}+\sqrt{z}(p-\sqrt{z})^2.$$

The integral in Eq. 21 can be written as

$$w_2(-z)\sim-\frac{i}{\pi}exp\left(-i\frac{2}{3}z^{3/2}\right)\int_0^\infty exp\left(i\sqrt{z}(p-\sqrt{z})^2\right)dp. \tag{22}$$

Assuming that the stationary point $\sqrt{z}$ is far from the integration limit $p = 0$, we can integrate from $-\infty$ to ∞. The result of the integration is

$$w_2(-z) \sim \frac{1}{\sqrt{\pi}} z^{-1/4} exp\left(-i\frac{2}{3}z^{3/2} - i\frac{\pi}{4}\right). \tag{23}$$

Using Eq. 23 we derive the asymptotics of Eq. 19, assuming $\left|\frac{t}{Y}\right| \ll 1$

$$w_2(t - Y) \sim \frac{1}{\sqrt{\pi}} Y^{-1/4} exp\left(-i\frac{2}{3}Y^{3/2} + it\sqrt{Y} - i\frac{1}{4}\frac{t^2}{\sqrt{Y}} - i\frac{\pi}{4}\right). \tag{24}$$

Therefore, the asymptotic representation for Eq. 20 assuming $|\alpha l^2 - t| \gg 1$ is the following

$$A_{asymp} = \frac{1}{\sqrt{\pi}} \alpha^{-1/4} l^{-1/2} exp\left(-it\sqrt{\alpha} r_c \vartheta - i\frac{t^2}{4\sqrt{\alpha l}} - i\frac{\pi}{4}\right). \tag{25}$$

This asymptotic solution is still the quasi-optical approximation. The term $exp\left(-i\frac{t^2}{4\sqrt{\alpha l}}\right)$ is responsible for diffusion across the rays. However, for the example under consideration the term, $\frac{t^2}{4\sqrt{\alpha l}}$, in Eq. 25 is small compared to the term, $t\sqrt{\alpha} r_c \vartheta$ and if we drop this term, we end up with the geometrical optics expression for the field.

Now, we apply the rigorous solution in the ray coordinates Eq. 20 and the asymptotic solution Eq. 25 to describe the radiation from the launcher.

The radiation is in the interval of angles $\vartheta_2 < \vartheta < \vartheta_1$ as shown in Fig. 3 where $\vartheta_2 = -\arccos\left(\frac{r_c}{a}\right)$ and $\vartheta_1 = \arccos\left(\frac{r_c}{a}\right)$ at $l = l_0 = \sqrt{a^2 - r_c^2}$, the field is uniform within the interval $\vartheta_2 < \vartheta < \vartheta_1$. We represent this field as a superposition of azimuthal harmonics

$$A_0(\vartheta) = \sum_{n=-\infty}^{n=\infty} C_n e^{-in\vartheta}. \tag{26}$$

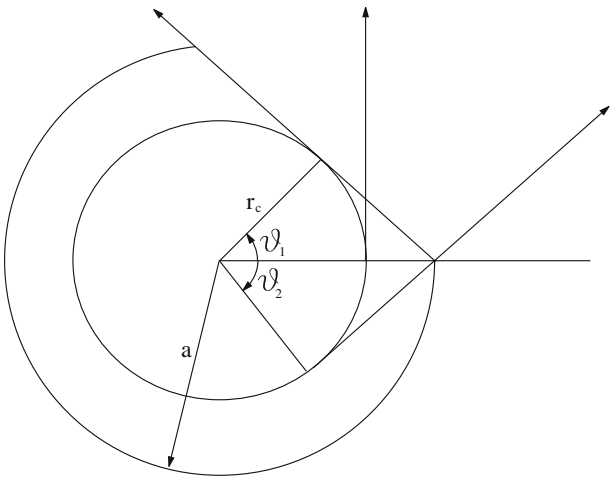

Fig. 3 The ray representation in the azimuthal plane.

The coefficients can be determined as follows

$$C_n = \frac{1}{2\pi}\int_0^{2\pi} A_0(\vartheta)e^{in\vartheta}\,d\vartheta$$
$$= \frac{1}{2\pi}\frac{e^{in\vartheta_1} - e^{in\vartheta_2}}{in} \tag{27}$$

for $n \neq 0$ and $C_0 = \frac{\vartheta_1 - \vartheta_2}{2\pi}$. Using Eq. 20, the radiated field, therefore, can be written as

$$A = \sum_{n=-N}^{n=N} C_n e^{-in\vartheta} e^{-i\frac{n}{r_c}(l-l_0)} \frac{w_2\left(\frac{n}{\sqrt{\alpha}r_c} - \alpha l^2\right)}{w_2\left(\frac{n}{\sqrt{\alpha}r_c} - \alpha l_0^2\right)} \cdot exp\left(i\frac{2}{3}\alpha^{3/2}(l^3 - l_0^3)\right). \tag{28}$$

This is the quasi-optical representation. Using Eq. 25, the asymptotic equation for the radiated field is now written as

$$A_{asymp} = \sum_{n=-N}^{n=N} \sqrt{\frac{l_0}{l}} C_n e^{-in\vartheta} exp\left(-i\frac{1}{4}\frac{n^2}{\alpha^{3/2}r_c^2}\left(\frac{1}{l} - \frac{1}{l_0}\right)\right). \tag{29}$$

The geometrical optics representation can be expressed as

$$A_{GO} = \sum_{n=-N}^{n=N} \sqrt{\frac{l_0}{l}} C_n e^{-in\vartheta}. \tag{30}$$

Equation 29 allows us to estimate the Fresnel parameter. At the aperture, the phase varies from 0 to $n\vartheta_1$, where $\vartheta_1 = \arctan\left(\frac{l_0}{r_c}\right)$. Let us assume $n\vartheta_1 \sim \pi$. Diffraction occurs if the phase in the second term varies by the same amount

$$\frac{n^2}{4\alpha^{3/2}r_c^2}\left(\frac{1}{l} - \frac{1}{l_0}\right) \sim \pi.$$

From $n\vartheta_1 \sim \pi$ and the above equation and using Eq. 14 we obtain

$$\frac{4\vartheta_1^2}{\lambda}\frac{ll_0}{l - l_0} \sim 1.$$

Introducing the aperture size $\sigma = l_0\vartheta_1$, we obtain the criterion of diffraction

$$N_F = \frac{4\sigma^2}{\lambda}\left(\frac{1}{l - l_0} + \frac{1}{l_0}\right) \sim 1,$$

where N_F is a generalized Fresnel parameter. $N_F \gg 1$ is the region of geometrical optics, $N_F \sim 1$ is the diffraction region.

4 Diffraction in axial plane

The radiation pattern of the launcher is three-dimensional and represented by the rays tangential to the cylindrical caustic $r = r_c$. However, we analyze the two-dimensional diffraction problem in the axial plane. In Fig. 3, this plane corresponds to the plane of central ray $\vartheta = 0$. The helical cut shown in Fig. 4 has a "visor" of the

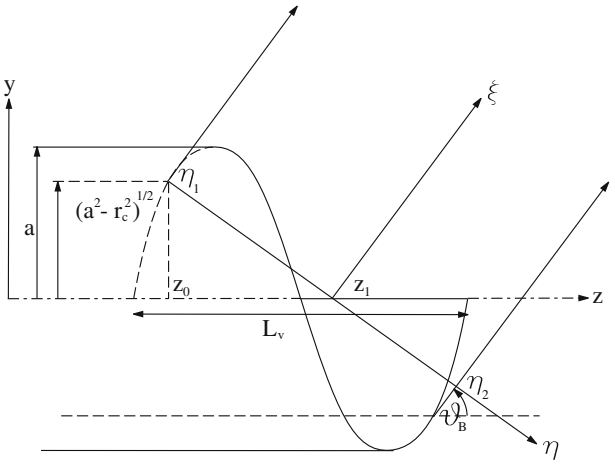

Fig. 4 The ray representation in the axial plane.

length of L_v. The axial plane (y, z) is parallel to the waveguide axis and intersects the waveguide at $y = \pm\sqrt{a^2 - r_c^2}$. The flow of rays is shown in Fig. 4 by the end rays.

The radiation is coming out at the bounce angle of $\vartheta_B = \arcsin\left(\frac{\nu}{ka}\right)$, ν is the root of the equation $J'_m(\nu) = 0$. We introduce the coordinates (ξ, η), where ξ is in the direction of rays and η is in the plane of the phase front,

$$\xi = (z - z_1)\cos\vartheta_B + y\sin\vartheta_B$$

$$\eta = (z - z_1)\sin\vartheta_B - y\cos\vartheta_B$$

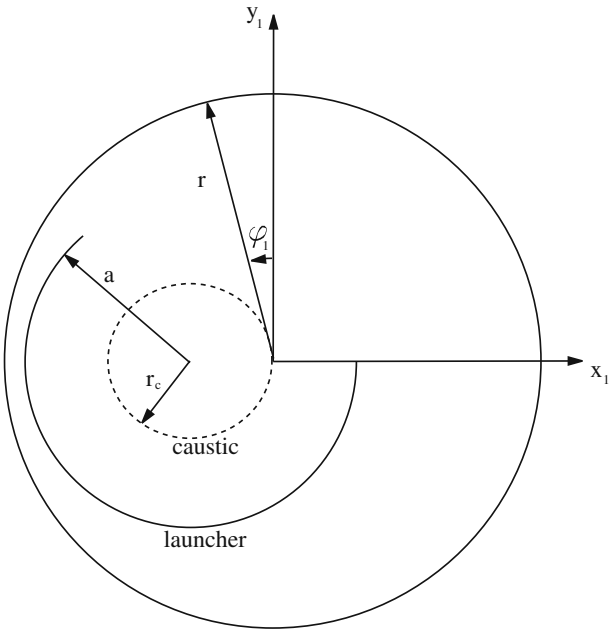

Fig. 5 Coordinates of the radiation pattern.

z_1 is the coordinate at which the phase front intersects the axis z

$$z_1 = z_0 + \sqrt{a^2 - r_c^2}\tan\vartheta_B.$$

The radiation field is described by the Helmholtz equation

$$\frac{\partial^2 u}{\partial \xi^2} + \frac{\partial^2 u}{\partial \eta^2} + k^2 u = 0. \tag{31}$$

which we represent in the quasi-optical approximation assuming k is a large parameter and $u = Ae^{-ik\xi}$

$$-2ik\frac{\partial A}{\partial \xi} + \frac{\partial^2 A}{\partial \eta^2} = 0. \tag{32}$$

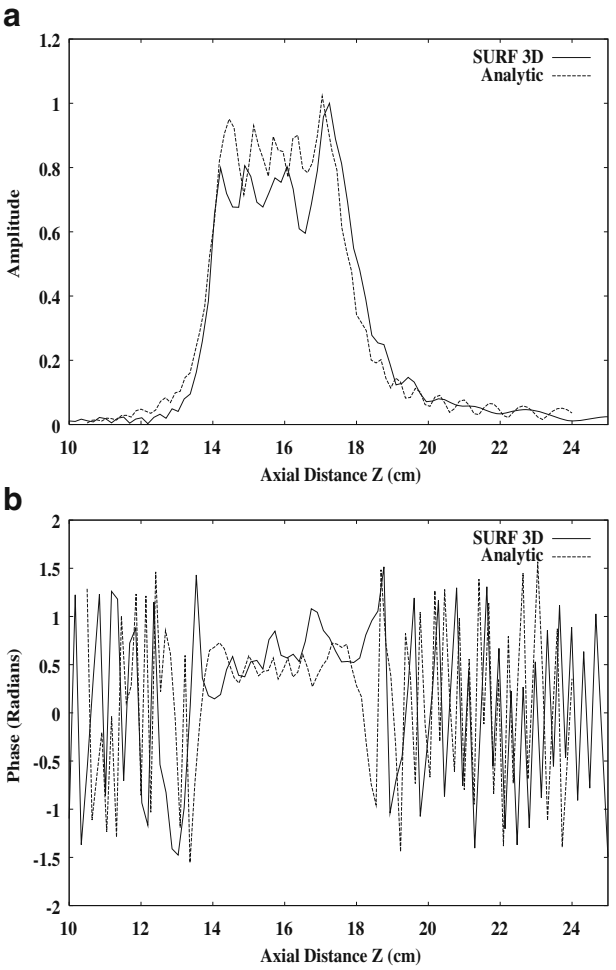

Fig. 6 **a** Amplitude and **b** phase along z at radius of cylinder 3.3 cm. (solid: SURF3D, dashed: analytic).

The parabolic equation Eq. 32 has the solution

$$A(\xi, \eta) = \int_{-\infty}^{\infty} A_0(\eta') G(\xi, \eta - \eta') d\eta', \tag{33}$$

where

$$G(\xi, \eta - \eta') = \frac{C}{\sqrt{\xi}} exp\left(-i\frac{k(\eta - \eta')^2}{2\xi}\right) \tag{34}$$

is a Green's function. $A_0(\eta) = A(0, \eta)$ is the complex amplitude at the plane $\xi = 0$. The constant C can be determined from the condition,

$$\lim_{\xi \longrightarrow 0} G(\xi, \eta - \eta') = \delta(\eta - \eta').$$

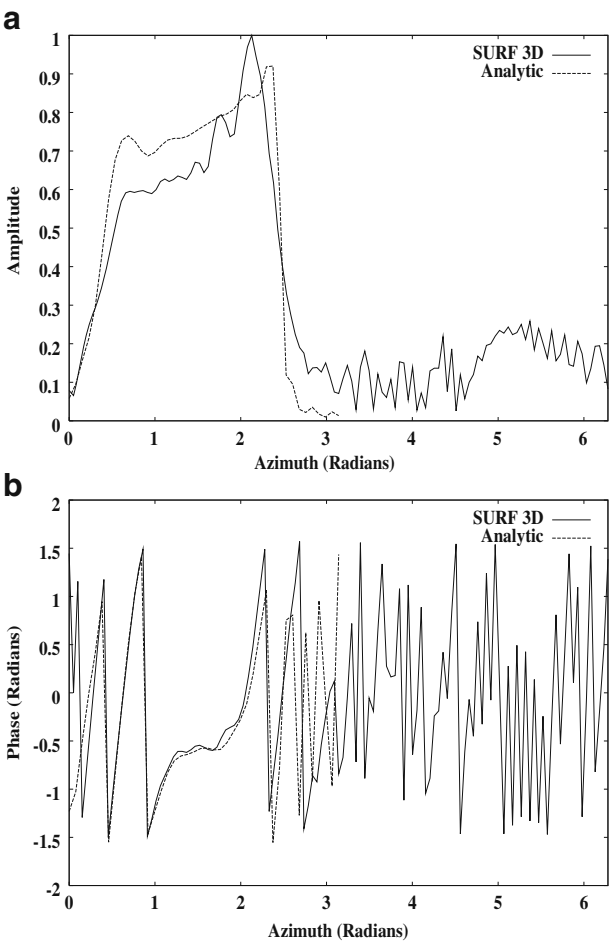

Fig. 7 **a** Amplitude and **b** phase along azimuth ϕ at radius of cylinder 3.3 cm. (solid: SURF3D, dashed: analytic).

Therefore

$$\frac{C}{\sqrt{\xi}}\int_{-\infty}^{\infty} exp\left(-i\frac{k\eta^2}{2\xi}\right)d\eta = \frac{C}{\sqrt{\xi}}\left(\frac{\pi}{i\frac{k}{2\xi}}\right)^{1/2} = 1$$

and $C = \sqrt{\frac{ik}{2\pi}}$. We assume $A_0(\eta) = 1$ in the interval $\eta_1 < \eta < \eta_2$, where

$$\eta_1 = -\frac{\sqrt{a^2 - r_c^2}}{\cos\vartheta_B}$$

and

$$\eta_2 = -\frac{\sqrt{a^2 - r_c^2}}{\cos\vartheta_B} + L_v \sin\vartheta_B.$$

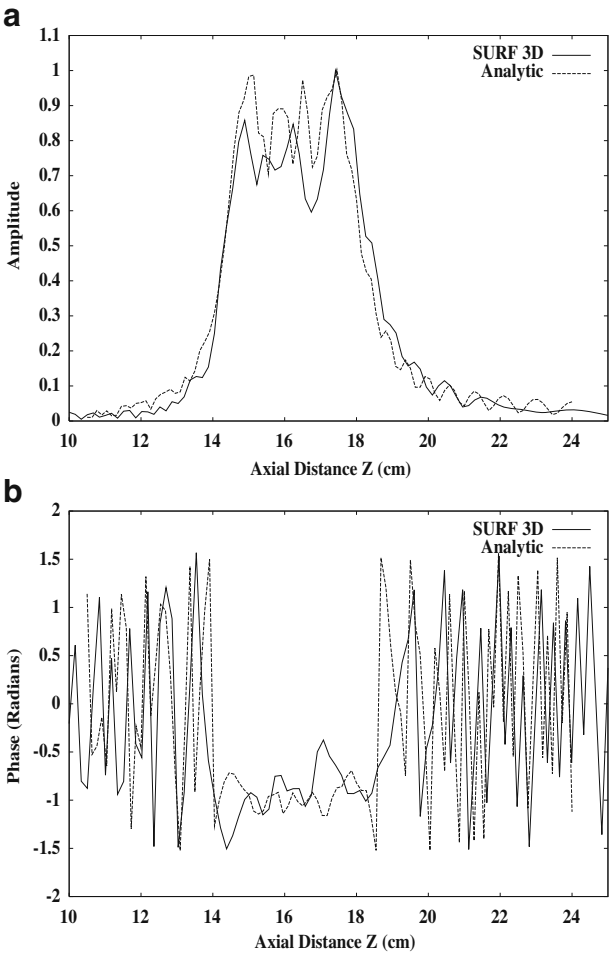

Fig. 8 **a** Amplitude and **b** phase along z at radius of cylinder 4 cm. (solid: SURF3D, dashed: analytic).

From Eqs. 33 and 34 we obtain

$$A(\xi,\eta) = \sqrt{\frac{ik}{2\pi\xi}} \int_{\eta_1}^{\eta_2} exp\left(-i\frac{k(\eta-\eta')^2}{2\xi}\right) d\eta'$$

$$= F\left(\sqrt{\frac{k}{2\xi}}(\eta_2-\eta)\right) - F\left(\sqrt{\frac{k}{2\xi}}(\eta_1-\eta)\right), \tag{35}$$

where the Fresnel integral is expressed as

$$F(x) = \sqrt{\frac{i}{\pi}} \int_{-\infty}^{x} e^{-it^2} dt. \tag{36}$$

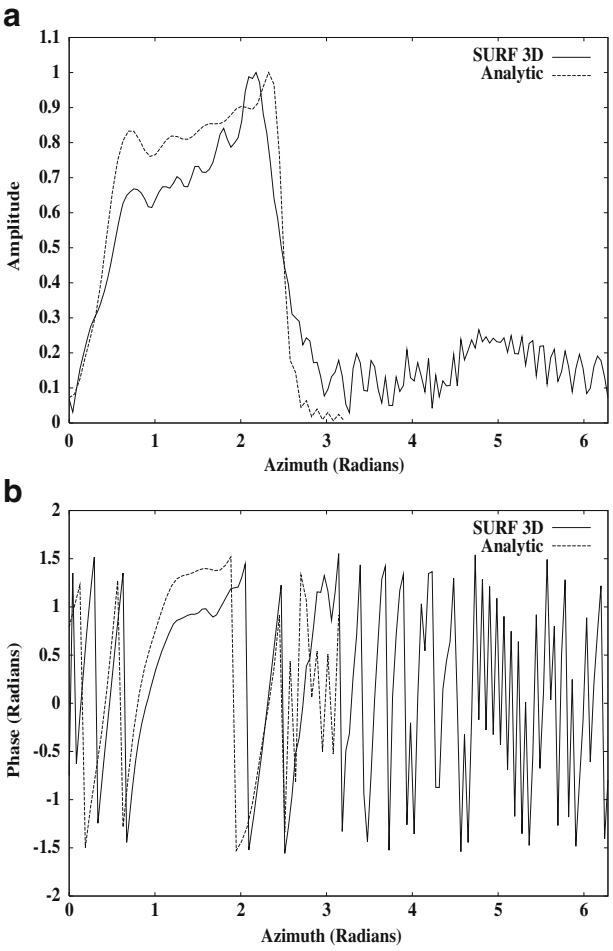

Fig. 9 **a** Amplitude and **b** phase along azimuth ϕ at radius of cylinder 4 cm. (solid: SURF3D, dashed: analytic).

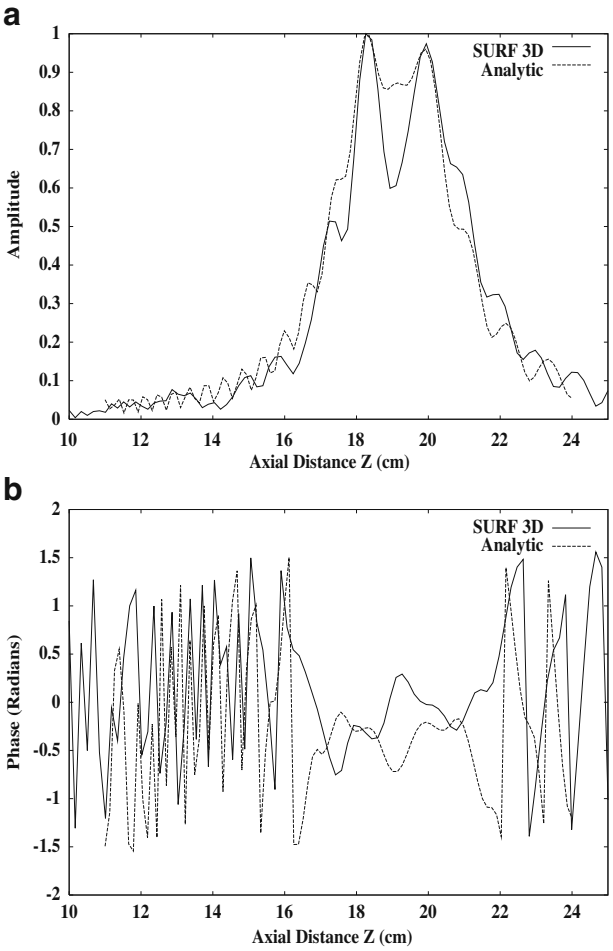

Fig. 10 **a** Amplitude and **b** phase along z at radius of cylinder 10 cm. (solid: SURF3D, dashed: analytic).

5 Example of calculation of the launcher radiation

We employ SURF3D, an electric field integral equation (EFIE) code [14], to propagate the radiation from the launcher to the cylinder which is shown in Fig. 5; (x_1, y_1) are the coordinates of the observation point. The axis of the cylinder z_1 is at the caustic. The launcher radius is $a = 2.1966$ cm. The caustic radius for the mode $\mathrm{TE}_{22,6}$ is $r_c = \frac{m}{\nu}a = 1.059$ cm and the transverse wave number is $k_\perp = \frac{\nu}{a} = 20.77\ \mathrm{cm}^{-1}$ where ν is 45.62, which is the 6-th zero of the derivative of Bessel function $J_m(x)$ with $m = 22$. Therefore, the angle ϑ varies from $\vartheta_2 = -\arccos\frac{r_c}{a} = -61.2°$ to $\vartheta_1 = 61.2°$. The parameter $\alpha = \left(\frac{k_\perp}{2r_c^2}\right)^{2/3} = 4.409\ \mathrm{cm}^{-2}$. The diffraction in the axial plane is calculated for the wave number $k = 23.05\ \mathrm{cm}^{-1}$ at the frequency f =110 GHz.

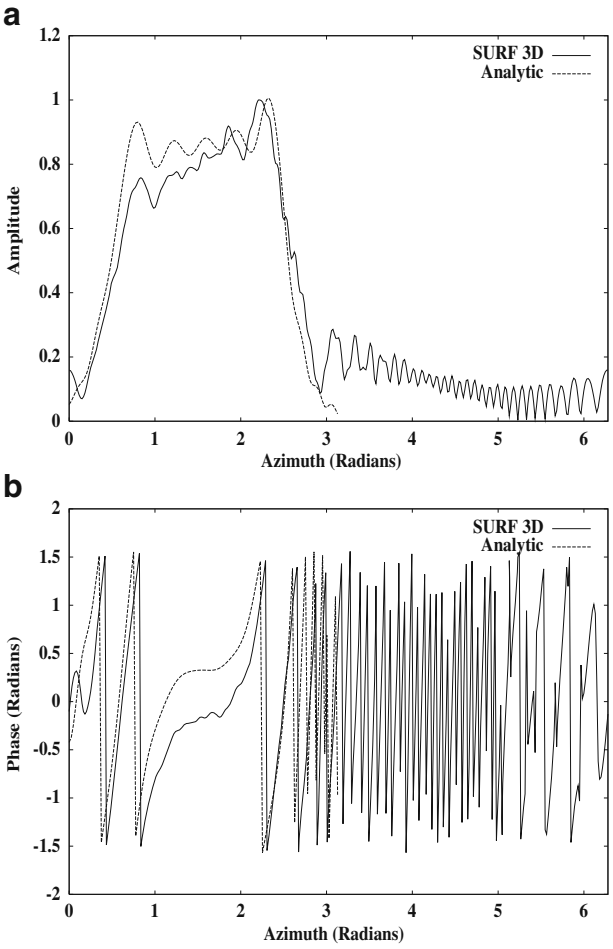

Fig. 11 **a** Amplitude and **b** phase along azimuth ϕ at radius of cylinder 10 cm. (solid: SURF3D, dashed: analytic).

In Eq. 28 we consider l and ϑ as functions of r_1 and φ_1

$$l = \sqrt{r_1^2 - 2r_1 r_c \sin\varphi_1} \tag{37}$$

$$\vartheta = \arccos\left(-\frac{r_1 \sin\varphi_1 - r_c}{\sqrt{l^2 + r_c^2}}\right) - \arccos\left(\frac{r_c}{\sqrt{l^2 + r_c^2}}\right). \tag{38}$$

The calculations have been carried out for $r_1 = 3.3,\ 4$, and 10 cm. Distributions of both amplitude and phase were calculated using SURF3D and compared to the equation Eq. 28. The number of azimuthal harmonics N in Eq. 28 was chosen to be 18 in the calculation. Figures 6, 7, 8, 9, 10, and 11 show the comparison between the SURF3D simulation and analytic solution at the measurement cylinder of radius of 3.3, 4, 10 cm.

We have found very good agreement between the quasi-optical representation of the radiation field and the numerical simulations. For the field distribution in the axial plane (y_1, z_1), the analytic results from the quasi-optical representation are plotted and compared to the numerical results in Figs. 6, 8, and 10. The visor length of $L_v = 4.1$ cm was used. It is slightly larger than twice the Brillouin length $2L_B$, where the Brillouin length $L_B = 2\sqrt{a^2 - r_c^2}\cot\vartheta_B = 1.83$ cm. According to the geometrical optics [10], such a launcher radiates in all directions in the azimuthal plane. It is shown in Figs. 7, 9, and 11 which plot the simulation results in the azimuthal planes. Figure 7 is plotted for the axial cross section at -1.8 cm from the launcher tip. It shows a sidelobe in the backward direction. Therefore, the visor length of this launcher is not optimized. The quasi-optical representation results match very well with the numerical results.

For the field distribution in the azimuthal plane, the results from (Eqs. 28, 29) are generated and the results show identical field patterns for both representations. This means that once the ray leaves the waveguide it is in the geometrical optics zone which extends all the way to infinity. The calculated Fresnel number is $N_F = 32$ at infinity and larger as we approach to the aperture of the waveguide cut. Only the quasi-optical results are plotted in Figs. 7, 9, and 11 and compared to the numerical results. The amplitude distributions in Figs. 7a, 9a, and 11a are plotted in the full region of the azimuthal direction which includes the light and dark regions. There is good agreement between the analytic results and numerical results in the light region. The amplitude distribution is not symmetrical which is consistent with geometrical optics. In fact, one side on the light region is closer to the aperture than the other. However the sidelobes are present in the amplitude plots in the numerical results whereas the analytic results do not show the sidelobes. The phase distributions presented in Figs. 7b, 9b, and 11b show also good agreement between the analytic theory and the numerical results. The phase flattens out in the light region surrounding the central ray according to the analytic representation. The phase becomes a fast varying function of the azimuthal coordinate outside the light region because the observation cylinder does not coincide with the phase front $s = const$.

6 Conclusions

We have found the quasi-optical solution for the diffraction of the rotating mode at a helical cut of a circular waveguide. SURF3D, a simulation code that solves the electric field integral equation (EFIE) is used to compare the analytic results with numerical simulations. The comparison between the SURF3D simulation and analytic solution will give a somewhat better understanding for the mode converter description. The result shows that the quasi-optical representation describes the radiation field qualitatively and gives reasonable quantitative information.

Acknowledgements The authors would like to thank J. Neilson for providing the SURF3D code, S. T. Han and Y. Hidaka for help with paper preparation. This research is supported by the U. S. Department of Energy, Office of Fusion Energy Sciences, and also by the National Institutes of Health (NIH) / National Institute for Biomedical Imaging and Bioengineering (NIBIB) (contracts EB001965 and EB004866).

References

1. G. S. Nusinovich, *Introduction to the Physics of Gyrotrons* (The Johns Hopkins University Press, Baltimore, 2004).
2. M. V. Kartikeyan, E. Borie, and M. K. A. Thumm, *Gyrotrons: High Power Microwave and Millimeter Wave Technology* (Springer, Berlin Heidelberg New York, 2004).
3. S. N. Vlasov, L. I. Zagryadskaya, and M. I. Petelin, "Transformation of a whispering gallery mode propagating in a circular waveguide into a beam of waves," Radio Eng. Electron. Phys. **20**, 14–17 (1975).
4. M. K. Hornstein, V. S. Bajaj, R. G. Griffin, K. E. Kreischer, I. Mastovsky, M. A. Shapiro, J. R. Sirigiri, and R. J. Temkin, "Second harmonic operation at 460 GHz and broadband continuous frequency tuning of a gyrotron oscillator," IEEE Trans. Electron Devices **52**, 798–807 (2005).
5. T. Idehara, I. Ogawa, S. Mitsudo, M. Pereyaslavets, N. Nishida, and K. Yoshida, " Development of frequency tunable medium power gyrotrons (gyrotron FU series) as submillimeter wave radiation sources," IEEE Trans. Plasma Sci. **27**, 340–354 (1999).
6. I. Ogawa, T. Idehara, M. L. Pereyaslavets, and W. Kasparek, "Design of quasi-optical systems converting a gyrotron output into a Gaussian-like beam," Int. J. Electron. **87**, 865–877 (2000).
7. J. A. Lorbeck, and R. J. Vernon, "Singly curved dual-reflector synthesis technique applied to a quasi-optical antenna for a gyrotron with a whispering-gallery mode output," IEEE Trans. Antennas Propag. **39**, 1733–1741 (1991).
8. S. N. Vlasov, and M. A. Shapiro, "Bievolvent mirror for transfer of caustic surfaces," Sov. Tech. Phys. Lett. **15**, 374 (1989).
9. S. N. Vlasov, M. A. Shapiro, and E. V. Sheinina, "Wave beam shaping on diffraction of a whispering gallery wave at a convex cylindrical surface," Radio Phys. Quant. Electron. **31**, 1070 (1988).
10. S. N. Vlasov, M. A. Shapiro, and K. M. Likin, "Geometrical optics of waveguide mode converters," Optics Commun. **88**, 455 (1992).
11. G. G. Denisov, A. N. Kuftin, V. I. Malygin, N. P. Venediktov, D. V. Vinogradov, and V. E. Zapevalov, "110 GHz gyrotron with built-in high efficiency converter," Int. J. Electron. **72**, 1079 (1992).
12. M. Iima, M. Sato, Y. Amano, S. Kobayashi, M. Nakajima, M. Hashimoto, O. Wada, K. Sakamoto, M. Shiho, T. Nagashima, M. Thumm, A. Jacobs, and W. Kasparek, "Measurement of radiation field from an improved efficiency quasi-optical converter for whispering-gallery mode," in *Conf. Digest, 14th Int. Conf. on Infrared and Millim. Waves, Wurzburg, Proc. SPIE 1240*, p. 405 (1989).
13. M. K. Thumm, and W. Kasparek, "Passive high-power microwave components," IEEE Trans. Plasma Sci. **30**, 755–786 (2002).
14. J. M. Neilson, and R. Bunger, "Surface integral equation analysis of quasi-optical launcher," IEEE Trans. Plasma Sci. **30**, 794 (2002).
15. H. Shirai, and L. B. Felsen, "Rays and modes for plane wave coupling into a large open-ended circular waveguide," Wave Motion **9**, 461–482 (1987).
16. V. M. Babich, and V. S. Buldyrev, *Short-wavelength Diffraction Theory: Asymptotic Methods* (Springer-Verlag, Berlin Heidelberg New York, 1991).
17. K. Goto, T. Ishihara, and L. B. Felsen, "High-frequency whispering-gallery mode to beam conversions on a perfectly conducting concave-convex boundary," IEEE Trans. Antennas Propag. **50**, 1109–1119 (2002).
18. V. A. Fock, *Electromagnetic Diffraction and Propagation Problems* (Pergamon Press, Oxford New York, 1965).
19. G. D. Malyuzhinets, and L. A. Vainshtein, "Transverse diffusion for diffraction at an impedance cylinder of large radius. I. Parabolic equation in ray coordinates," Radiotekh. Elektron. **6**, 1247–1258 (1961).
20. S. Solimeno, B. Crosignani, and P. DiPorto, *Guiding, Diffraction, and Confinement of Optical Radiation* (Academic Press, Orlando, 1986).